

LOCALIZED DISPERSIVE STATES IN NONLINEAR COUPLED MODE EQUATIONS FOR LIGHT PROPAGATION IN FIBER BRAGG GRATINGS*

C. MARTEL[†], M. HIGUERA[†], AND J.D. CARRASCO[†]

Abstract. Dispersion effects induce new instabilities and dynamics in the weakly nonlinear description of light propagation in fiber Bragg gratings. A new family of dispersive localized pulses that propagate with the group velocity is numerically found and its stability is also analyzed. The unavoidable different asymptotic order of transport and dispersion effects plays a crucial role in the determination of these localized states. These results are also interesting from the point of view of general pattern formation since this asymptotic imbalance is a generic situation in any transport dominated (i.e., nonzero group velocity) spatially extended system.

1. Introduction. Fiber Bragg gratings (FBG) are microstructured optical fibers that present a spatially periodic variation of the refractive index. The combination of the guiding properties of the periodic media with the Kerr nonlinearity of the fiber results in the very particular light propagation characteristic of these elements, which make them very promising for many technological applications that range from optical communications (wavelength division, dispersion management, optical buffers and storing devices, etc.) to fiber sensing (structural stress measure in aircraft components and buildings, temperature change detection, etc.), see, e.g., the recent review [8].

The amplitude equations that are commonly used in the literature to model one dimensional light propagation in a FBG are the so-called nonlinear coupled mode equations (NLCME) [17, 6, 5, 1, 7], which, conveniently scaled, can be written as

$$A_t^+ - A_x^+ = i\kappa A^- + iA^+(\sigma|A^+|^2 + |A^-|^2), \quad (1.1)$$

$$A_t^- + A_x^- = i\kappa A^+ + iA^-(\sigma|A^-|^2 + |A^+|^2), \quad (1.2)$$

where A^\pm are the envelopes of the two counterpropagating wavetrains that resonate with the grating, κ is the strength of the coupling effect produced by the grating and $\sigma > 0$ is ratio of the self to cross nonlinear interaction coefficient ($\sigma = \frac{1}{2}$ for a cubic Kerr nonlinearity [6]). The NLCME can be obtained from the full Maxwell-Lorentz equations using multiple scales techniques in the limit of small grating depth, small light intensity and slow spatial and temporal dependence of the field envelopes (see [7] for a detailed description of this derivation process).

It has been recently shown [11, 12] that light propagation in FBG can develop dispersive structures that are not accounted for in the NLCME formulation, and that, to correctly describe the weakly nonlinear dynamics of the system, the NLCME have to be completed with material dispersion terms:

$$A_t^+ - A_x^+ = i\kappa A^- + iA^+(\sigma|A^+|^2 + |A^-|^2) + i\varepsilon A_{xx}^+, \quad (1.3)$$

$$A_t^- + A_x^- = i\kappa A^+ + iA^-(\sigma|A^-|^2 + |A^+|^2) + i\varepsilon A_{xx}^-. \quad (1.4)$$

The dispersive nonlinear coupled mode equations above (NLCME_d) are scaled as the NLCME: the characteristic length scale is the slow scale that results from the balance

*This work was supported by Spanish Direcci3n General de Investigaci3n under grant MTM2004-03808 and by the Universidad Polit3cnica de Madrid under grant CCG06-UPM/IME-328.

[†]Depto. de Fundamentos Matem3ticos, E.T.S.I. Aeron3uticos, Universidad Polit3cnica de Madrid, Plaza Cardenal Cisneros 3, 28040 Madrid, SPAIN (martel@fmetsia.upm.es, maria@fmetsia.upm.es, carrasco@fmetsia.upm.es).

of the advection term with the small effect of the grating, the characteristic time is the corresponding transport time scale (which sets to one the scaled group velocity), and the characteristic size of the wavetrains is the resulting one from the saturation of the small nonlinear terms. The slow envelope assumption forces the dispersive terms to be always small as compared with the advection terms; in other words, second derivatives of the slow amplitudes are much smaller than first derivatives. In the scaled equations this effect is contained in the scaled dispersion coefficient ε (which measures the dispersion to transport ratio) and therefore, in order to be consistent with the slow envelope assumption, the NLCMED must be considered in the limit $\varepsilon \rightarrow 0$.

The NLCMED can be somehow regarded as asymptotically nonuniform, in the sense that the NLCMED is an asymptotic model obtained in the $\varepsilon \rightarrow 0$ (weakly nonlinear, slow envelope) limit that still contains the small parameter ε . This is the unavoidable consequence of simultaneously considering two balances of different asymptotic order: one induced by the dominant effect of the transport at the group velocity (balance described by NLCME) and a second one that is associated with the underlying dispersive, nonlinear Schrödinger-like dynamics of the system. The small dispersive terms in the NLCMED are essential to describe the dynamics of the system when it develops small dispersive scales $\delta_{\text{disp}} \sim \sqrt{|\varepsilon|}$. As it was shown in [11], the NLCMED in the $\varepsilon \rightarrow 0$ limit constitute a singular perturbation problem (cf. [10]) and the onset of the dispersive scales is not a higher order, longer time effect; it takes place in the same timescale of the NLCME, no matter how small is the dispersion coefficient ε .

A solution of the NLCMED for $\varepsilon = -10^{-3}$ that exhibits small dispersive scales all over the domain is represented in Figure 1.1: note that, for short time, the dispersive structures just propagate with the group velocity but, for $t \sim 1$, they also interact with each other giving rise to a very complicated spatio-temporal pattern. The initial condition used in this simulation was a uniform modulus solution with a small random perturbation that, according to the dispersion-less NLCME formulation, was a stable solution. In order to ensure that the small scales in Figure 1.1 are dispersion induced scales we have repeated the NLCMED simulation but with a reduced dispersion $\varepsilon = -10^{-3}/4$. The result is plotted in Figure 1.2 where it can be seen that the small scales fill again the entire domain, but its typical size, $\delta_{\text{disp}} \sim \sqrt{|\varepsilon|}$, is now approximately one half of that in Figure 1.1 (see also the corresponding animations `movie1.1.gif` and `movie1.2.gif`).

The main goal of this paper is to show that, in addition to complex spatio-temporal patterns, the dispersion effects can also give rise to new, purely dispersive localized states, which might be of interest from the optical communications point of view. It is interesting to note that the results in this paper apply also to Bose-Einstein condensates in optical lattices (a system that has recently received very much attention [15, 18]) and, in general, to any dissipation-less propagative system, extended in one spatial direction, reflection and translation invariant, and with a small superimposed spatial periodic modulation of its background, since the NLCMED are the appropriate envelope equations for the description of the weakly nonlinear resonant dynamics of this kind of systems.

In order to show that light propagation in a FBG can happen in the form of dispersive pulses, we derive and solve numerically in section 2 an asymptotic equation for a family of symmetric pulses, and, in section 3, we perform some numerical integrations of the complete NLCMED to show that some of the pulses in this family do

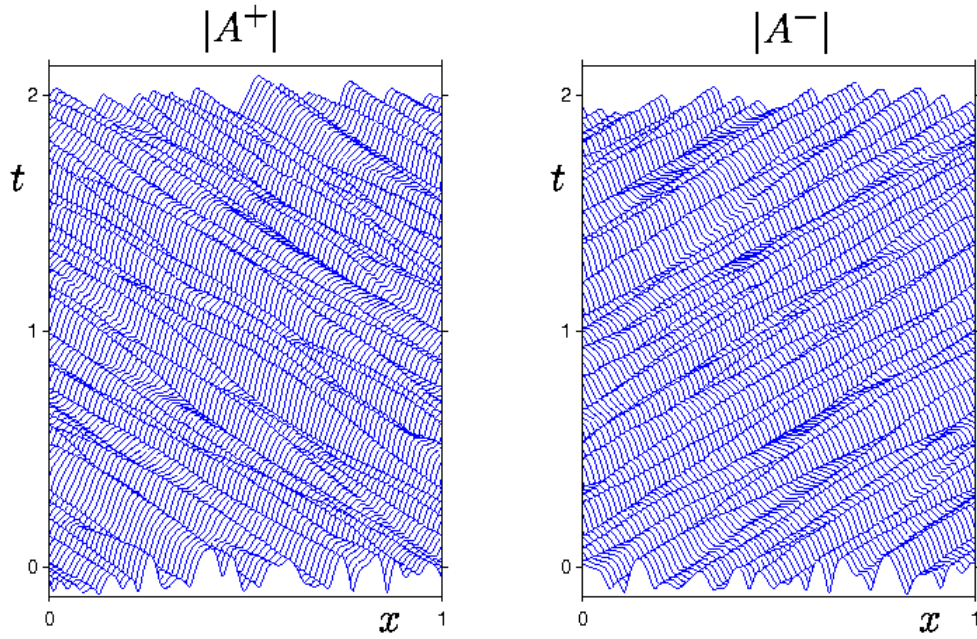


FIG. 1.1. Space-time representation of a solution of the NLCMEd exhibiting small dispersive scales all over the domain ($\sigma = 1/2$, $\kappa = 2$, $\varepsilon = -10^{-3}$, and periodicity boundary conditions). See the file `movie1.1.gif` for an animation of the onset of the dispersive scales.

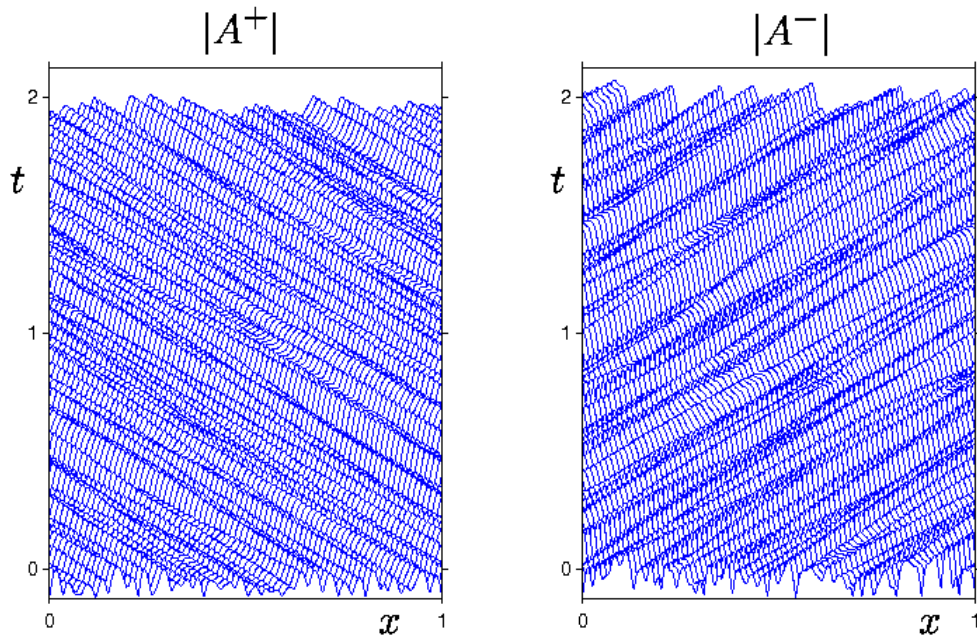


FIG. 1.2. Space-time representation of a solution of the NLCMEd exhibiting small dispersive scales all over the domain ($\sigma = 1/2$, $\kappa = 2$, $\varepsilon = -10^{-3}/4$, and periodicity boundary conditions). See the file `movie1.2.gif` for an animation of the onset of the dispersive scales.

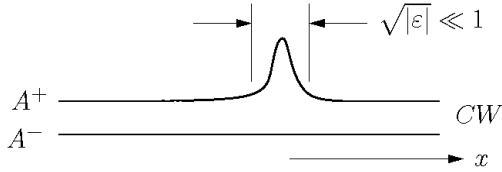


FIG. 2.1. Sketch of a dispersive pulse on top of a continuous wave.

propagate as stable localized structures. Finally, some concluding remarks are drawn in section 4.

2. Dispersive pulses. The starting point is the continuous wave (CW) family of constant uniform modulus solutions of the NLCME (1.1)-(1.2)

$$A_{\text{CW}}^+ = \rho \cos \theta e^{i\omega t + imx}, \quad (2.1)$$

$$A_{\text{CW}}^- = \rho \sin \theta e^{i\omega t + imx}, \quad (2.2)$$

where $\rho \geq 0$ is the light intensity flowing through the fiber, $\theta \in [-\frac{\pi}{2}, \frac{\pi}{2}]$ measures the relative amount of both wavetrains, and the frequency and wavenumber of the amplitudes are given by

$$\omega = \frac{\kappa}{\sin 2\theta} + \frac{\sigma + 1}{2} \rho^2, \quad (2.3)$$

$$m = \left(\frac{\kappa}{\sin 2\theta} - \frac{\sigma - 1}{2} \rho^2 \right) \cos 2\theta. \quad (2.4)$$

The CW with $|\omega| \sim 1$ and $|m| \sim 1$ are approximate solutions of the NLCMEd (up to order ε corrections) and its stability was first analyzed in [5] and then completed in [11], where it was found that, for both signs of the dispersion coefficient, there are dispersively unstable CW which are stable in the dispersion less context of the NLCME.

We now look for localized dispersive pulses propagating on top of one of the amplitudes of a stable CW, as sketched in Figure 2.1. In order to turn the background CW into a constant, it is convenient to first perform in the NLCMEd the following change of variables

$$\begin{aligned} A^+ &= F^+ e^{i\omega t + imx}, \\ A^- &= F^- e^{i\omega t + imx}, \end{aligned}$$

to obtain

$$F_t^+ - F_x^+ + i(\omega - m)F^+ = i\kappa F^- + iF^+(\sigma|F^+|^2 + |F^-|^2) + i\varepsilon F_{xx}^+, \quad (2.5)$$

$$F_t^- + F_x^- + i(\omega + m)F^- = i\kappa F^+ + iF^-(\sigma|F^-|^2 + |F^+|^2) + i\varepsilon F_{xx}^-. \quad (2.6)$$

A localized dispersive pulse on F^+ depends on the fast spatial scale $X = x/\sqrt{|\varepsilon|}$ and, according to (2.5)-(2.6), in the short time scale, $T = t/\sqrt{|\varepsilon|} \sim 1$, it just propagates with the group velocity, suggesting that we have to look for solutions of the form

$$\begin{aligned} F^+ &= F_0^+(\eta, t) + \dots, \\ F^- &= F_0^-(\eta, t) + \dots, \end{aligned}$$

with $\eta = X + T$. Inserting the above ansatz into (2.5)-(2.6) yields

$$F_{0\eta}^- = 0, \quad \text{that gives} \quad F_0^- = \rho \sin \theta,$$

which means that F^- remains in first approximation equal to the unperturbed CW. Similarly, the following equation is obtained for F_0^+

$$F_{0t}^+ + i(\omega - m)F_0^+ = i\kappa\rho \sin \theta + iF_0^+(\sigma|F_0^+|^2 + \rho^2 \sin^2 \theta) \pm iF_{0\eta\eta}^+, \quad (2.7)$$

where the $+$ ($-$) sign corresponds to ε positive (negative), together with the boundary conditions

$$F_0^+ \rightarrow \rho \cos \theta \quad \text{for} \quad \eta \rightarrow \pm\infty, \quad (2.8)$$

which ensure that the background CW is recovered away from the pulse.

For dispersive pulses propagating over a zero background we have to set to zero ρ , ω and m in eq. (2.7). A standard nonlinear Schrödinger (NLS) equation is then obtained, which is known to exhibit localized pulses (solitons) in the focusing case of positive dispersion (recall that $\sigma > 0$). Note that in this case the effect of the grating is completely gone because it takes place only through the background state. The only nonzero Fourier spectrum components of these NLS solitons correspond, in first approximation, to very large dispersive wavenumbers ($\sim 1/\sqrt{|\varepsilon|} \gg 1$) that are so off-resonance that they simply do not feel the grating.

Equation (2.7) is a nonlinear Schrödinger equation with a direct forcing term coming from the effect of the grating. The steady solutions of this equation and their stability properties were analyzed in [2, 3], where explicit analytic expressions for the steady pulses were found. In this paper we consider the more general family of traveling localized solutions. More precisely, we look for traveling pulses of the form

$$F_0^+ = \rho \cos \theta(1 + a(\eta + vt)),$$

where v represents, in the original variables, a small correction of the group velocity. The resulting boundary value problem for a , after making use of relations (2.3) and (2.4) and the rescaled variable $\xi = (\eta + vt)(\sqrt{\sigma}\rho \cos \theta)$, can be written as

$$a_{\xi\xi} = -i\hat{v}a_{\xi} + \alpha a - (|a|^2 + a + \bar{a})(1 + a), \quad (2.9)$$

$$a \rightarrow 0 \quad \text{as} \quad \xi \rightarrow \pm\infty \quad (2.10)$$

where $\hat{v} = v/(\sqrt{\sigma}\rho \cos \theta)$ and $\alpha = k \tan(\theta)/(\sigma\rho^2 \cos^2 \theta)$. We are restricting our search to the focusing case of positive sign in eq. (2.7) and, in order to have a dispersively stable background CW, we have to consider only the range $0 < \theta < \frac{\pi}{2}$ (see [11]), which implies that we have to look for pulses in eqs. (2.9)-(2.10) only for $\alpha > 0$. On the other hand, eqs. (2.9)-(2.10) remain invariant under the transformation $\hat{v} \rightarrow -\hat{v}$ and $a \rightarrow \bar{a}$, and therefore we can also set $\hat{v} \geq 0$.

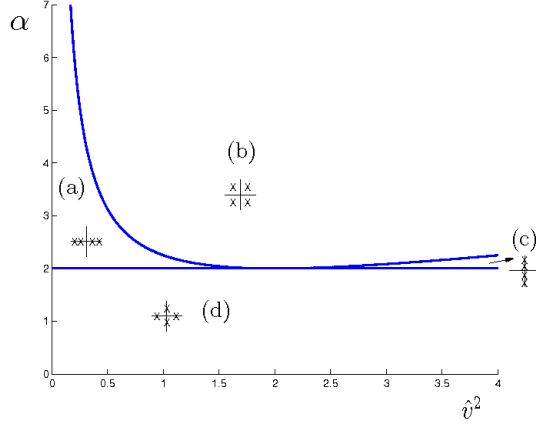


FIG. 2.2. Eigenvalues of the trivial state as a function of the parameters α and \hat{v}^2 . Sketches show the distribution of the four eigenvalues in each of the distinct regions.

The solutions of eqs. (2.9)-(2.10) correspond to traveling dispersive pulses and can be regarded as homoclinic orbits (in the variable ξ) connecting the trivial state (i.e., $a = 0$) back to itself.

To analyze the existence of such connections we first consider the linearized system around the zero state:

$$\frac{d\mathbf{u}}{d\xi} = A_\infty \mathbf{u} \quad (2.11)$$

where $\mathbf{u}^T \equiv (a_r, a_i, (a_r)_\xi, (a_i)_\xi)$, a_r and a_i are the real and imaginary part of a , $(a_r)_\xi = da_r/d\xi$ and $(a_i)_\xi = da_i/d\xi$, and the matrix A_∞ is given by

$$A_\infty = \begin{pmatrix} 0 & 0 & 1 & 0 \\ 0 & 0 & 0 & 1 \\ \alpha - 2 & 0 & 0 & \hat{v} \\ 0 & \alpha & -\hat{v} & 0 \end{pmatrix}. \quad (2.12)$$

The eigenvalues of this system are given by $\lambda_\pm^1 = \sqrt{\eta_\pm}$ and $\lambda_\pm^2 = -\sqrt{\eta_\pm}$, with

$$\eta_\pm = \left[2\alpha - (\hat{v}^2 + 2) \pm \sqrt{(\hat{v}^2 + 2)^2 - 4\hat{v}^2\alpha} \right] / 2. \quad (2.13)$$

Fig. 2.2 shows the behaviour of the four eigenvalues λ_\pm^1 and λ_\pm^2 in the (α, \hat{v}^2) plane. There are four distinct regions, separated by the boundaries $\alpha = 2$ and $\alpha = (\hat{v}^2 + 2)^2 / 4\hat{v}^2$: (a) four real eigenvalues, (b) two pairs of complex conjugate eigenvalues, (c) four purely imaginary eigenvalues and (d) two real eigenvalues along with two purely imaginary eigenvalues. In regions (a) and (b) the unstable and stable manifolds of the origin are two dimensional, while the equilibrium is nonhyperbolic in regions (c) and (d) where the center manifold is, respectively, four- and two-dimensional. Homoclinic orbits belong to both the stable and unstable manifold of the origin. We investigate below the presence of homoclinic solutions in cases (a) and (b), where these correspond to the intersections of two dimensional stable and unstable manifolds in a four dimensional space [16].

The problem (2.9)-(2.10) is invariant under the symmetry

$$a \rightarrow \bar{a}, \quad \xi \rightarrow -\xi, \quad (2.14)$$

that comes from the time reversing (Hamiltonian) and spatial reflection symmetries of the NLCMEd. We further restrict our search for dispersive pulses to the case of reflection-symmetric pulses, i.e., to pulses that satisfy:

$$a(\xi) = \bar{a}(-\xi).$$

If we now set the symmetry axis to $\xi = 0$, we can reduce the problem to a semi-infinite interval $\xi \in [0, +\infty[$ with the boundary conditions

$$(a_r, a_i) = (a_0, 0) \quad \text{and} \quad ((a_r)_\xi, (a_i)_\xi) = (0, b_0), \quad \text{at} \quad \xi = 0, \quad (2.15)$$

$$(a_r, a_i) \rightarrow (0, 0) \quad \text{as} \quad \xi \rightarrow \infty. \quad (2.16)$$

Finally, to numerically compute the profiles of the symmetric pulses, we replace the infinite interval by a finite one, $[0, L]$. Following [9], the resulting boundary conditions at $\xi = L$ are obtained by requiring that the solution projects only onto the subspace spanned by the eigenvectors associated with the decaying eigenvalues of the matrix A_∞ (see eq. (2.11)). In summary, the boundary value problem that we integrate numerically is given by eq. (2.9), which we rewrite as a real first order system of four equations in $]0, L[$ together with the four boundary conditions

$$C_0 \mathbf{u} = \mathbf{0} \quad \text{at} \quad \xi = 0, \quad \text{and} \quad (2.17)$$

$$C_\infty \mathbf{u} = \mathbf{0} \quad \text{at} \quad \xi = L, \quad (2.18)$$

where $\mathbf{u}^T \equiv (a_r, a_i, (a_r)_\xi, (a_i)_\xi)$,

$$C_0 = \begin{pmatrix} 0 & 1 & 0 & 0 \\ 0 & 0 & 1 & 0 \end{pmatrix}, \quad (2.19)$$

and C_∞ is a matrix whose rows are the left eigenvectors of A_∞ associated with the exponentially growing directions

$$C_\infty = \begin{pmatrix} (\eta_+ - \alpha - \hat{v}^2) & \alpha \hat{v} / \sqrt{\eta_+} & (\eta_+ - \alpha) / \sqrt{\eta_+} & \hat{v} \\ (\eta_- - \alpha - \hat{v}^2) & \alpha \hat{v} / \sqrt{\eta_-} & (\eta_- - \alpha) / \sqrt{\eta_-} & \hat{v} \end{pmatrix}, \quad (2.20)$$

For each value of α this problem is solved using a shooting method. We start from the known solutions for $\hat{v} = 0$ obtained in [3] and apply numerical continuation techniques to locate the propagating pulses with $\hat{v} > 0$. This procedure for setting the boundary conditions at $\xi = L$, rather than simply imposing $a(L) = 0$, allows the shooting method to converge faster, and the results obtained are found to be essentially independent of L for $L \gtrsim 10$.

The left panel of Fig. 2.3 shows several families of homoclinic orbits represented in the (a_0, \hat{v}) plane for different values of α and corresponding to the case $a_0 > 0$. The dashed line separates the regions where the homoclinic orbit connects to a saddle point, and where it connects to a saddle-focus, while the open circles correspond to the solutions shown on the right panels. In Fig. 2.3 II a-c the solutions can be seen to develop oscillations as we move towards $a_0 = 0$. This corresponds to moving along a horizontal line in Fig. 2.2 (constant α) and to the right, approaching region (c) (precisely at $a_0 = 0$, $\hat{v} = \sqrt{\alpha} + \sqrt{\alpha - 2}$) where the eigenvalues become purely imaginary.

This oscillatory behaviour, however, is not observed for the families of pulse solutions found for $a_0 < 0$, as seen in Fig. 2.4. Instead, these curves display turning

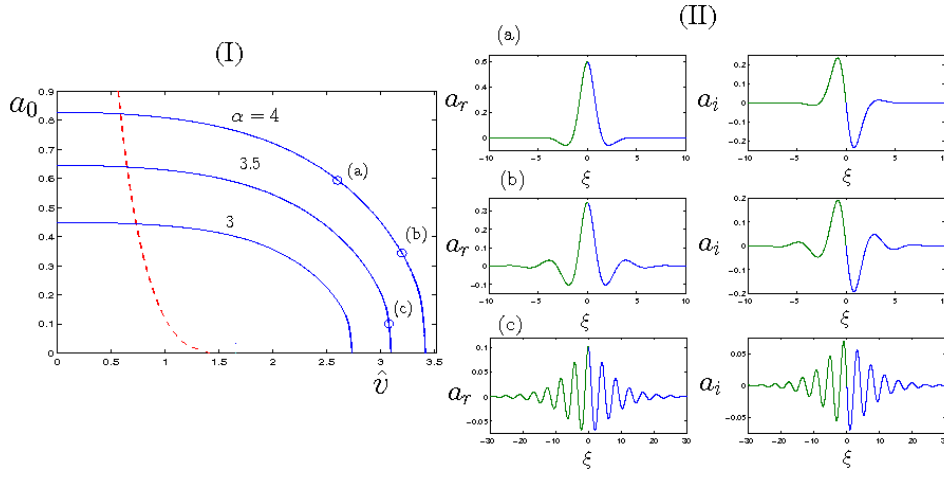


FIG. 2.3. (I) The solid lines correspond to homoclinic cycles to the origin with $a_0 > 0$ for the indicated values of α . The dashed line bounds the regions where the origin is a saddle node (on the left) and saddle-focus (on the right). (II) Spatial profiles of three pulses for the values marked in (I) with open circles.

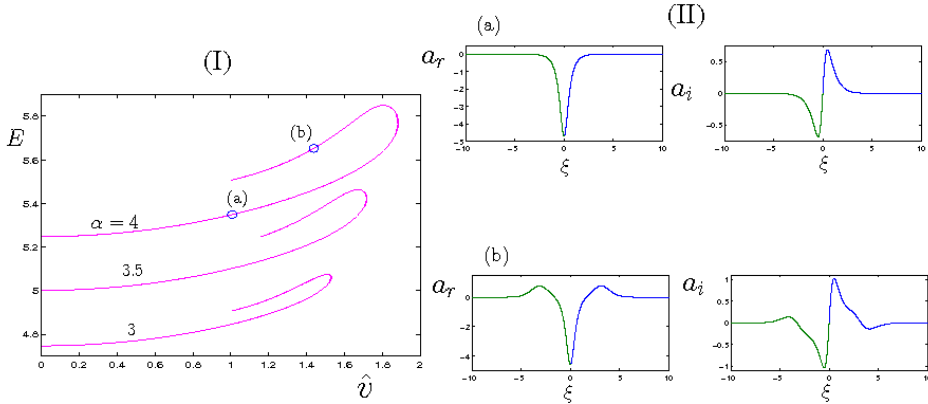


FIG. 2.4. (I) Curves of homoclinic cycles to the origin with $a_0 < 0$ for the indicated values of α . (II) Spatial profiles of two pulses corresponding to the values marked in (I) with open circles.

points and, to better appreciate these limit points, the results have been plotted in the plane (E, \hat{v}) , where E is the positive quantity

$$E = \sqrt{\int_0^\infty (|a|^2 + |a_\xi|^2) d\xi}.$$

In this case, as we move along the curves for fixed α and past the turning point, the pulses develop two extra humps that tend to move away from the origin (see Fig. 2.4 II (a) and (b)).

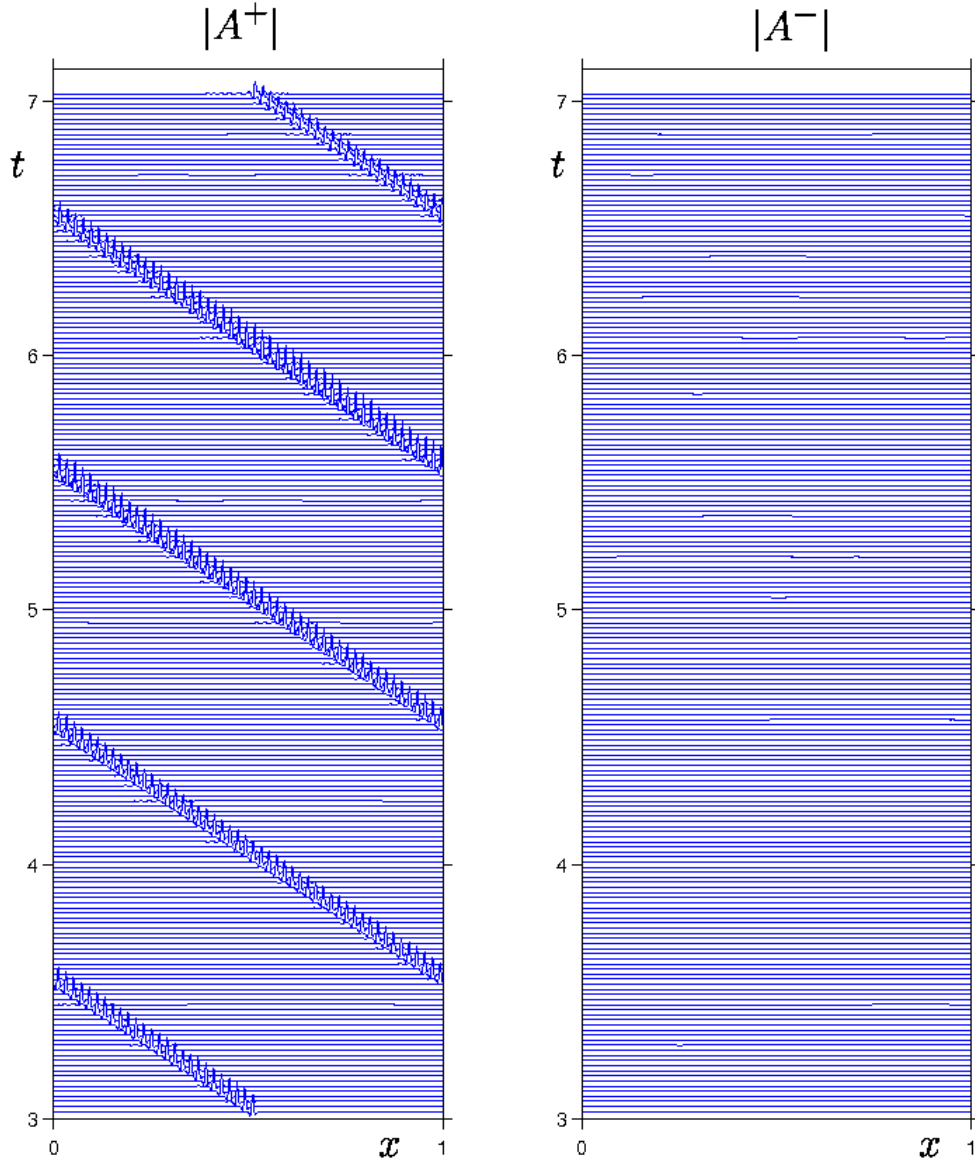


FIG. 3.1. Space-time representation of the solution of the NLCMEd ($\sigma = 1/2$, $\kappa = 1$, $\varepsilon = 10^{-5}$, and periodicity boundary conditions) for a unstable pulse propagating on top of a CW ($\rho = 1$ and $\theta = \pi/4$). The pulse parameters are $\alpha = 4$ and $\hat{v} = 1$, and it corresponds to the point labeled (a) in Fig. 2.4. See the file `movie3.1.gif` for an animation of this pulse destabilization.

3. NLCMEd simulations. After having found a two parameter (α, \hat{v}) family of symmetric dispersive pulses (DP) that can be numerically continued from the solutions for $\hat{v} = 0$ obtained in [3], we now proceed to study their stability.

The idea is not to perform a complete stability analysis of the family of DP but to show that stable DP can be found, and that the DP can thus be considered as robust realizable localized structures of light propagation in FBG. To do this we select several DP, place them on top of their corresponding background CW, add a small random perturbation, and use them as initial conditions for the full system of NLCMEd (1.3-1.4) that we numerically integrate for a certain amount of time with periodic boundary conditions. The numerical method for the integration of the NLCMEd uses a Fourier series in space with N_F modes and a fourth order Runge-Kutta scheme for the time integration of the resulting system of ordinary differential

equations for the Fourier coefficients. The stiff linear diagonal terms associated with the small dispersion coefficients are integrated implicitly, and the nonlinear terms are computed in physical space with the usual 2/3 rule to avoid the aliasing effects [4] (the maximum required resolution for the simulations in this paper were $N_F = 4096$ and $\Delta t = .0005$).

Unstable DP simply do not persist and their shape changes, as it can be appreciated from the spatio-temporal evolution shown in Fig. 3.1, which corresponds to the pulse labeled (a) in Fig. 2.4 (see also the corresponding animation `movie3.1.gif`). Note that the size of the pulse grows, at $t = 5.5$ it is larger than at $t = 3$, and then it decays again at $t = 7.0$. A few time units later the oscillatory tails spread and the pulse structure is eventually lost (not shown in the Figure). All DP explored for $a_0 < 0$ propagated over the same simple CW with parameters $\rho = 1$ and $\theta = \pi/4$ (cf. eqs. (2.1)-(2.2)), which corresponds to $\alpha = 4$ in eq. (2.14), and all were found to be unstable regardless of its propagation speed \hat{v} .

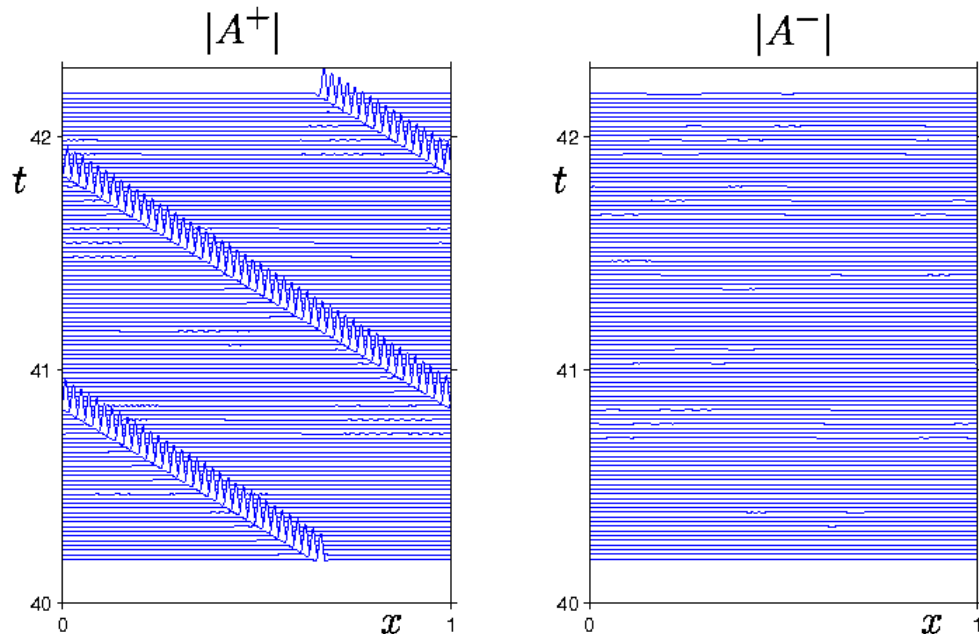


FIG. 3.2. Space-time representation of the solution of the NLCMEd ($\sigma = 1/2$, $\kappa = 1$, $\varepsilon = 10^{-5}$, and periodicity boundary conditions) for a stable pulse propagating on top of a CW ($\rho = 1$ and $\theta = \pi/4$). The pulse parameters are $\alpha = 4$ and $\hat{v} = 2.6$, and it corresponds to the point labeled (a) in Fig. 2.3. See the file `movie3.2.gif` for an animation of this propagating pulse.

On the other hand, for $a_0 > 0$ and for the same background CW (i.e., $\alpha = 4$), the DP are found to be unstable approximately for $0 \leq \hat{v} \lesssim 2.2$ and stable for $v \gtrsim 2.2$. The evolution of two stable pulses is shown in Figs. 3.2 and 3.3, which correspond to $\hat{v} = 2.6$ and $\hat{v} = 3.2$, respectively, where the structure of the slightly perturbed pulses is seen to remain now virtually unaltered after more than 40 time units (see also the corresponding animations `movie3.2.gif` and `movie3.3.gif`).

Another very interesting feature of the DP that is worth mentioning is the fact that they are somehow transparent to each other: two DP propagating in opposite directions just pass through each other without distortion. This is illustrated in Fig. 3.4 (see also the animation `movie3.4.gif`) where two stable DP (corresponding

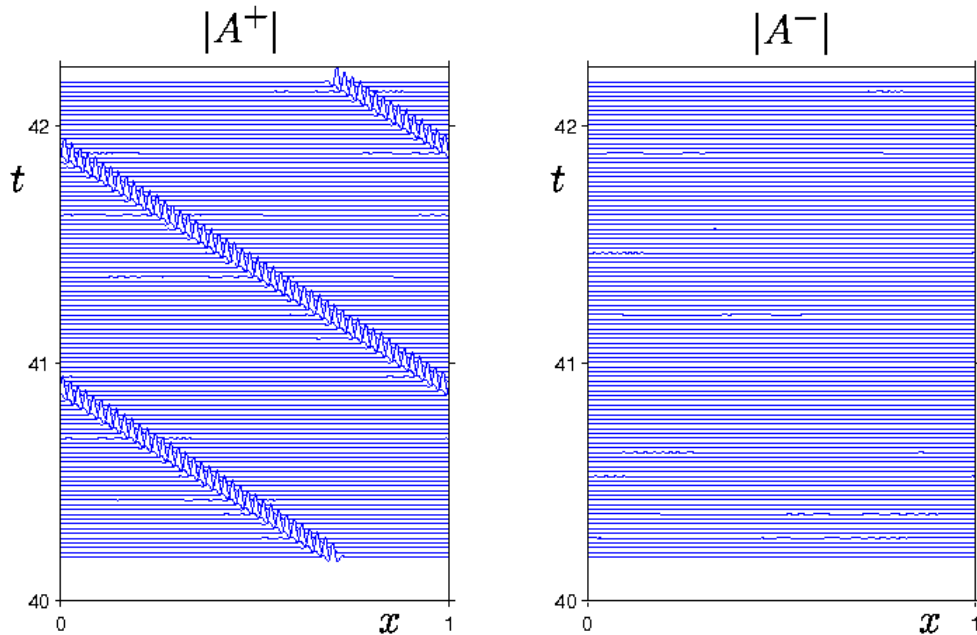


FIG. 3.3. Space-time representation of the solution of the NLCMEd ($\sigma = 1/2$, $\kappa = 1$, $\varepsilon = 10^{-5}$, and periodicity boundary conditions) for a stable pulse propagating on top of a CW ($\rho = 1$ and $\theta = \pi/4$). The pulse parameters are $\alpha = 4$ and $\hat{v} = 3.2$, and it corresponds to the point labeled (b) in Fig. 2.3. See the file `movie3.3.gif` for an animation of this propagating pulse.

to those in Figs. 3.2 and 3.3) are sent towards each other and after 40 time units (approximately 80 collisions) they still remain practically undistorted. The reason of this behavior is the dominant character of the transport effect induced by the group velocity. If we rewrite the NLCMEd for a DP with short (dispersive) spatial and temporal scales $X = x/\sqrt{\varepsilon} \sim 1$ and $T = t/\sqrt{\varepsilon} \sim 1$, they take the form of two uncoupled wave equations

$$\begin{aligned} A_T^+ &= A_X^+ + \dots, \\ A_T^- &= -A_X^- + \dots, \end{aligned}$$

and then it is clear that DP travelling in opposite directions simply propagate through different channels, and are (in first approximation) completely independent.

4. Conclusions. In this paper we have studied the effect of dispersion in the weakly nonlinear dynamics of light propagation in a FBG. We have shown that the (often neglected) small dispersion terms play a crucial role in the transport dominated dynamics of light propagation in FBG. Dispersion can give rise to complex spatio-temporal chaotic states, but also to a new family of localized states (DP) that propagate over a CW background and do not interact with each other. These DP are approximately advected by the group velocity, but this transport effect does not play any role in the determination of their internal structure, which results basically from a balance between nonlinearity and dispersion. It is also important to emphasize that this type of dynamics is not contained in the standard dispersion-less NLCME formulation for light propagation in FBG. Moreover, this behavior is just the result of the competition of two effects with different asymptotic order: transport and disper-

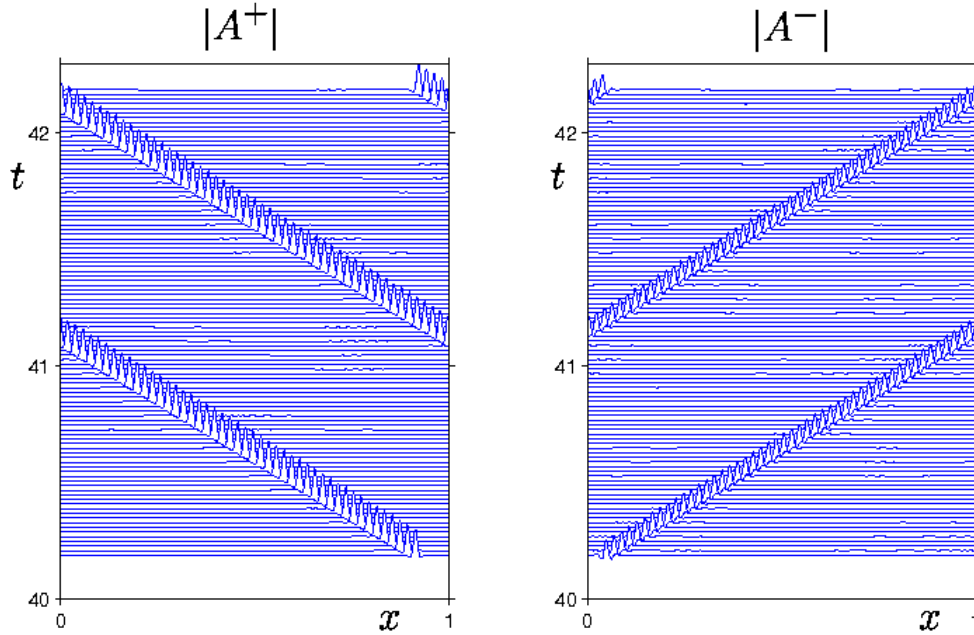


FIG. 3.4. Space-time representation of the solution of the NLCMEd ($\sigma = 1/2$, $\kappa = 1$, $\varepsilon = 10^{-5}$, and periodicity boundary conditions) showing the simultaneous propagation in opposite directions of the two stable pulses from Figs. 3.2 and 3.3. See the file `movie3.4.gif` for an animation of this pulse interaction.

sion, and this is a generic situation that applies to any propagative extended system unless some special care is taken to reduce the group velocity (similar effects have been previously described in the context of Hopf bifurcation in dissipative systems [13] and in parametrically forced surface waves [14]).

REFERENCES

- [1] A.B. ACEVES, *Optical gap solitons: Past, present and future; theory and experiment*, CHAOS, 10 (2000), pp. 584–589.
- [2] I.V. BARASHENKOV AND YU. S. SMIRNOV, *Existence and stability chart for the ac-driven, damped nonlinear schrodinger solitons*, Phys. Rev. E, 54 (1996), pp. 5707–5725.
- [3] I.V. BARASHENKOV, T. ZHANLAV, AND M.M. BOGDAN, *Instabilities and soliton structures in the driven nonlinear schrodinger equation*, in Nonlinear World vol. 1, Proceedings of the IV International Workshop on Nonlinear and Turbulent Processes in Physics, V.G. Bar'yakhtar, V.M. Chernousenko, N.S. Erokhin, A.G. Sitenko, and V.E. Zakharov, eds., World Scientific, 1989.
- [4] C. CANUTO, H.Y. HUSSANI, A. QUARTERONI, AND T.A. ZANG, *Spectral Methods in Fluid Mechanics*, Springer Series in Computational Physics, Springer-Verlag, 1988.
- [5] C.M. DE STERKE, *Theory of modulational instability in fiber bragg gratings*, J. Opt. Soc. Am. B, 15 (1998), pp. 2660–2667.

- [6] C.M. DE STERKE AND J.E. SIPE, *Gap solitons*, Progress in Optics, XXXIII (1994), pp. 203–260.
- [7] R.H. GOODMAN, M.I. WEINSTEIN, AND P.J. HOLMES, *Nonlinear propagation of light in one-dimensional periodic structures*, J. Nonlinear Sci., 11 (2001), pp. 123–168.
- [8] RAMAN KASHYAP, *Fiber Bragg Gratings*, Optics and Photonics, Academic Press, 1999.
- [9] H.B. KELLER, *Numerical solution of two point boundary value problems*, vol. 24 of CBMS-NSF Regional Conferences in Applied Mathematics, SIAM, 1976.
- [10] J. KEVORKIAN AND J.D. COLE, *Multiple Scale and Singular Perturbation Methods*, vol. 114 of Applied Mathematical Sciences, Springer-Verlag, 1996.
- [11] C. MARTEL, *Dispersive destabilization of nonlinear light propagation in fiber bragg gratings*, CHAOS, 15 (2005), p. 013701.
- [12] C. MARTEL AND C.M. CASAS, *Dispersive destabilization of nonlinear light propagation in fiber bragg gratings: a numerical verification*, CHAOS, 17 (2007), p. 013114.
- [13] C. MARTEL AND J.M. VEGA, *Dynamics of a hyperbolic system that applies at the onset of the oscillatory instability*, Nonlinearity, 11 (1998), pp. 105–142.
- [14] C. MARTEL, J.M. VEGA, AND E. KNOBOCH, *Dynamics of counterpropagating waves in parametrically driven systems: dispersion vs. advection*, Physica D, 174 (2003), pp. 198–217.
- [15] H. SAKAGUCHI AND B.A. MALOMED, *Dynamics of positive- and negative-mass solitons in optical lattices and inverted traps*, J. Phys. B: At. Mol. Opt. Phys., 37 (2004), pp. 1443–1459.
- [16] S. WIGGINS, *Global Bifurcation and Chaos*, vol. 73 of Applied Mathematics Series, Springer-Verlag, 1988.
- [17] H.G. WINFUL AND G.D. COOPERMAN, *Self-pulsing and chaos in distributed feedback bistable optical devices*, Appl. Phys. Lett., 40 (1982), pp. 298–300.
- [18] A.V. YULIN AND D.V. SKRYABIN, *Out-of-gap bose-einstein solitons in optical lattices*, Phys. Rev. E, 67 (2003), p. 023611.